ISIJ International, Vol. 59 (2019), No. 9, pp. 1573–1581

Practical Operation Guidance on Thermal Control of Blast Furnace

Yoshinari HASHIMOTO,[1)]* Yuki OKAMOTO,[2)] Tatsuya KAISE,[2)] Yoshitaka SAWA[3)] and Manabu KANO[4)]

1) Instrument and Control Engineering Research Department, Steel Research Laboratory, JFE Steel Corp, Fukuyama, 721-8510 Japan.
2) Ironmaking Department, Fukuyama Works, JFE Steel Corp, Fukuyama, 721-8510 Japan.
3) JFE Techno-Research Corp., Kawasaki, 210-0855 Japan.
4) Department of Systems Science, Graduate School of Informatics, Kyoto University, Kyoto, 606-8501 Japan.

(*Received on February 26, 2019; accepted on April 12, 2019*)

Blast furnaces are still manually operated in the steel industry. To realize an efficient and stable operation, the authors developed an operation guidance system for controlling hot metal temperature and applied it to actual furnaces. The system features a newly developed 2D transient model that describes the sluggish and complicated process dynamics. Based on the transient model, nonlinear model predictive control (NMPC) and moving horizon estimation (MHE) were adopted to provide operators with appropriate control actions while minimizing the undesirable influence of disturbances. The online validation results demonstrated that the developed operation guidance system successfully reduced the variance of HMT by 1.9°C.

KEY WORDS: nonlinear model predictive control; hot metal temperature; moving horizon estimation; process control; industrial application.

1. Introduction

Steel industry is largely responsible for the emission of CO_2, 70% of which stems from the blast furnace process where iron ore is reduced and smelted. In the recent operation, low reducing agent ratio (RAR) has been oriented in order to reduce the amount of CO_2, and it decreases the operational margin. In addition, fluctuations in the quality of raw materials are expected to increase in the long term since high-quality materials are being depleted. These trends make the stable operation of the blast furnace even more difficult.

Figure 1 shows the outline of a blast furnace, where the coke and the iron ore are loaded from the top of the furnace, and the hot metal and its viscous byproduct, *i.e.* the slag, are drained from the tap holes at the bottom. Control of hot metal temperature (HMT) is important to realize an efficient and stable operation of the blast furnace. The drainage of slag becomes extremely difficult when HMT is too low. On the other hand, unnecessary fuel is consumed when HMT becomes excessively high. Decreasing the variations in HMT makes it possible to lower the target value of HMT and RAR without impairing the furnace productivity.

Table 1 shows the classification of the variables in this paper. HMT is generally controlled by pulverized coal ratio (PCR), coke ratio (CR), and blast moisture (BM). In normal operation, HMT is controlled so that its deviation from the set point is less than 5°C. **Figure 2** shows the instance of large HMT variation caused by operators' excessive manipulations. The top figure shows PCR, which is mean centered. The bottom figure shows the control error of HMT, *i.e.* the deviation from the set point. The operators decreased PCR from 3.3 day to 3.8 day in response to the increase of HMT. This manipulation turned out to be excessive because the actual HMT was below the set point by 50°C around 4.3 day.

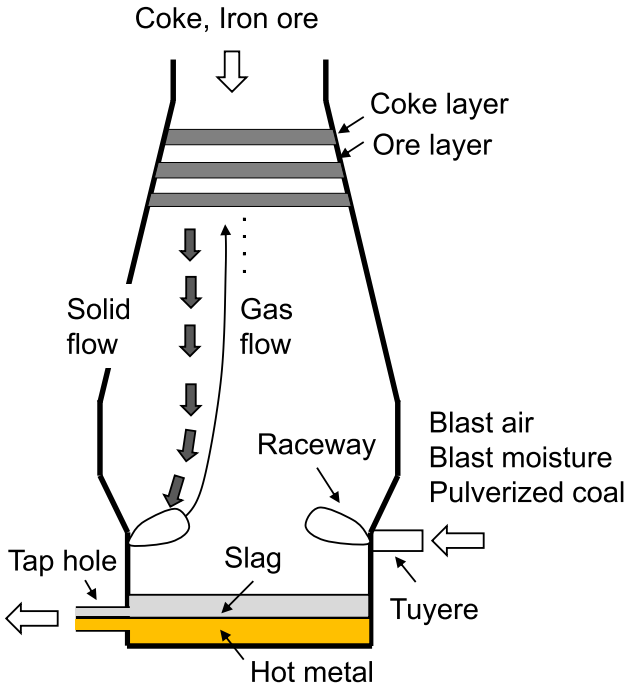

Fig. 1. Outline of blast furnace. (Online version in color.)

* Corresponding author: E-mail: y-hashimoto@jfe-steel.co.jp
DOI: https://doi.org/10.2355/isijinternational.ISIJINT-2019-119

The large heat capacity of the furnace lengthens the response time of HMT to the control actions. Moreover, it takes about six hours for the material charged from the top of the furnace to descend to the lower part of the furnace. Because of such slow process dynamics, the operators are not able to fully predict the effect of the manipulations and tend to perform excessive manipulations.

To perform appropriate manipulations while considering the long response time, a control law involving future state prediction is effective. It is to be desired that the control law is easily understood by the operators. Hence, this research aims at developing an operation guidance system using nonlinear model predictive control (NMPC)[1–4] to reduce the HMT variation. The NMPC algorithm adopted a new 2D transient model to predict the future HMT. In addition, we adopted moving horizon estimation (MHE)[5–7] which adjusts model parameters successively to minimize the undesirable influence of disturbances on the prediction.

The thermal control of blast furnace is known to be a challenging task in the field of process control of the steel industry. Many approaches have been proposed besides the transient model-based predictive control. HMT was predicted by a fuzzy inference system[8] or a data-based online model.[9] Silicon content of hot metal was predicted by a neural network model,[10] switching linear systems,[11] a non-Gaussian local regression,[12] a support vector regression,[13] or a just-in-time model.[14] Predictive control of silicon content with a neural network model[15] or a state-space model[16] was proposed. However, only a few studies have evaluated the performance of the control system in real plants. This research applied the transient model-based operation guidance system to the actual operation and validated its effect of reducing the HMT variance.

The outline of this paper is as follows. The new 2D transient model is described in section 2. Then, section 3 presents the NMPC algorithm using the 2D transient model. The operation guidance system based on NMPC is evaluated in section 4. Concluding remarks are given in section 5.

Table 1. Classification of variables in this work.

Variable	Dimension
Input variable for simulations	
Blast volume	[Nm^3/min]
Blast temperature	[°C]
Blast moisture (BM)	[g/Nm^3]
Pulverized coal (PC) flow rate	[kg/min]
Coke ratio (CR), *i.e.* weight ratio of coke and iron	[kg/t]
Enrichment oxygen	[Nm^3/min]
Top gas pressure	[kPa]
Manipulated variable for control	
Pulverized coal ratio (PCR), *i.e.* pulverized coal per iron	[kg/t]
Controlled variable	
Hot metal temperature (HMT)	[°C]

2. Development and Validation of 2D Transient Model

This section presents the 2D transient model and its validation using real plant data. Various blast furnace models have been proposed so far: for example, 1D steady-state model,[17] 1D transient model,[18–21] 2D steady-state model,[22–25] 2D transient model,[26,27] and 3D transient model.[28] The 1D transient models have been adopted in the model predictive control of HMT. In recent years, the radial distribution of ore-to-coke ratio at the furnace top is controlled to ensure the gas permeability. However, such radial distribution cannot be described in the 1D models. In addition, the fixed calculation cells reproducing the material layers in the furnace was employed in the conventional models except for our 1D transient model.[19] Numerical diffusion is caused by adopting the fixed calculation cells, which gives rise to the calculation error in transient states. To take account of the radial distribution of the ore-to-coke ratio while preventing the numerical diffusion, a new 2D transient model was developed in this work.

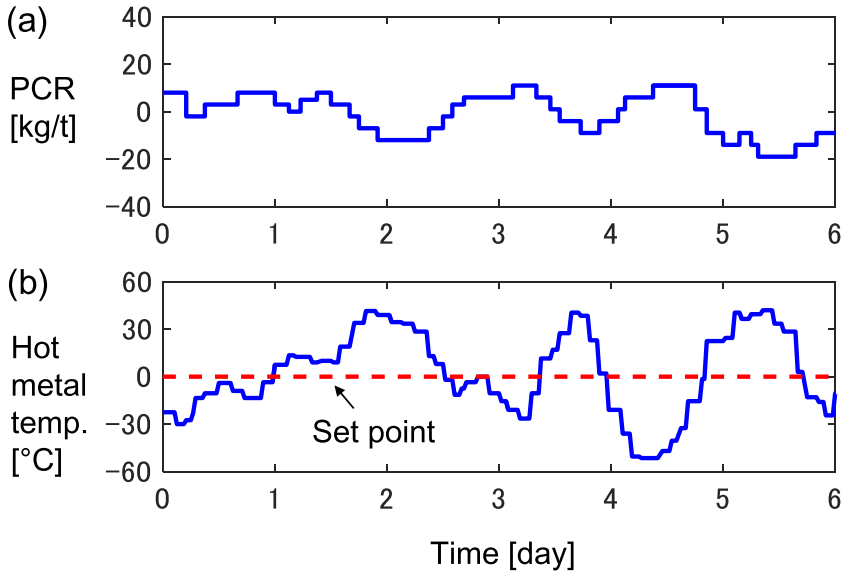

Fig. 2. Real operation data of manipulated variable PCR and controlled variable HMT. (Online version in color.)

2.1. Model Formulation and Solution Method

The axisymmetric 1D transient model[19] was expanded to the 2D transient model that involves four sub-models: a gas flow model, a reaction model, an energy balance model, and a solid flow model. The input variables in Table 1 were used to perform the simulation. The 12 reactions in **Table 2** are taken into account. The variables in the 2D transient model are summarized in **Table 3**.

The energy balance model that describes the convection heat transfer, the reaction heat, and the heat exchange between the solid and the gas is as follows.

$$\frac{\partial\left(\rho_{\mathrm{g}}C_{p,\mathrm{g}}T_{\mathrm{g}}\right)}{\partial t}+\nabla\cdot\left(C_{p,\mathrm{g}}T_{\mathrm{g}}\mathbf{u}_{\mathrm{g}}\right) = \sum_{j}\eta_{\mathrm{g}_j}\Delta H_{\mathrm{R}_j}R_j + E_{\mathrm{g,fe}}\left(T_{\mathrm{fe}}-T_{\mathrm{g}}\right)+E_{\mathrm{g,c}}\left(T_{\mathrm{c}}-T_{\mathrm{g}}\right)+q \quad \ldots (1)$$

Table 2. Reactions in 2D transient model.

Symbol	Notes
R_1	$FeO_x+CO=FeO_{x-1}+CO_2$
R_2	$C+CO_2=2CO$
R_3	$FeO+C=Fe+CO$
R_4	$FeO_x+H_2=FeO_{x-1}+H_2O$
R_5	$C+H_2O=CO+H_2$
R_6	$CO+H_2O=CO_2+H_2$
R_7	C(coke)=[C]
R_8	$SiO_2+2C=[Si]+2CO$
R_9	$H_2O(liq)=H_2O(g)$
R_{10}	$CaCO_3=CaO+CO_2$
R_{11}	$C+1/2O_2=CO$ (Raceway)
R_{12}	$C+H_2O=CO+H_2$ (Raceway)

Table 3. Variables in 2D transient model.

Symbol	Notes	Dimension
$C_{p,\mathrm{c}}$	Specific heat of coke	[J/kg·K]
$C_{p,\mathrm{g}}$	Specific heat of gas	[J/kg·K]
$C_{p,\mathrm{fe}}$	Specific heat of iron	[J/kmol·K]
E	Heat exchange coefficient	[J/m^3·s·K]
h	Overall heat transfer coefficient	[J/m^3·s·K]
R	Reaction rate	[kmol/m^{3}bed·s]
R_{c}	Consumption rate of coke	[kgcoke/m^{3}bed·s]
R_{o}	Melting rate of iron	[kmolFe/m^{3}bed·s]
u_{g}	Mass velocity of gas	[kg/m^2·s]
u_{fe}	Molar flux of liquid iron	[kmolFe/m^2·s]
q	Heat-loss through furnace wall	[J/m^3·s]
T	Temperature	[K]
X_{c}	Volume ratio of coke	[m^{3}coke/m^{3}bed]
X_{o}	Volume ratio of ore	[m^{3}ore/m^{3}bed]
ΔH_{R}	Reaction heat	[J/kmol]
η	Distribution ratio of reaction heat	[–]
ρ_{g}	Density of gas	[kg/m^3]
ρ_{c}	Apparent coke density	[kgcoke/m^{3}coke]
ρ_{fe}	Iron density in iron ore	[kmolFe/m^{3}ore]

$$\frac{\partial\left(\rho_{\mathrm{c}}C_{p,\mathrm{c}}X_{\mathrm{c}}T_{\mathrm{c}}\right)}{\partial t} = \sum_{j}\eta_{\mathrm{c}_j}\Delta H_{\mathrm{R}_j}R_j + E_{\mathrm{g,c}}\left(T_{\mathrm{g}}-T_{\mathrm{c}}\right)+E_{\mathrm{fe,c}}\left(T_{\mathrm{fe}}-T_{\mathrm{c}}\right) \quad \ldots (2)$$

$$\frac{\partial\left(\rho_{\mathrm{fe}}C_{p,\mathrm{fe}}X_{\mathrm{o}}T_{\mathrm{fe}}\right)}{\partial t}+\nabla\cdot\left(C_{p,\mathrm{fe}}T_{\mathrm{fe}}\mathbf{u}_{\mathrm{fe}}\right) = \sum_{j}\eta_{\mathrm{fe}_j}\Delta H_{\mathrm{R}_j}R_j + E_{\mathrm{g,fe}}\left(T_{\mathrm{g}}-T_{\mathrm{fe}}\right)+E_{\mathrm{fe,c}}\left(T_{\mathrm{c}}-T_{\mathrm{fe}}\right) \quad \ldots (3)$$

where the subscripts g, c, and fe represent gas, coke, and iron. The subscript j denotes the indices of the reactions. q is the heat flux through the furnace wall, *i.e.* heat-loss.

$$q=-h\left(T_{\mathrm{g}}-T_{\mathrm{w}}\right) \quad \ldots (4)$$

where h is the overall heat transfer coefficient to describe the heat flux from the bosh gas to the cooling water, and T_{w} is the cooling water temperature. This heat sink was incorporated in Eq. (1) as a source term.

The iron density in iron ore ρ_{fe} and the apparent density of coke ρ_{c} are calculated from the consumption rates of iron ore and coke, respectively.

$$X_{\mathrm{o}}\frac{\partial\rho_{\mathrm{fe}}}{\partial t}=-R_{\mathrm{o}} \quad \ldots (5)$$

$$\left(1-X_{\mathrm{o}}\right)\frac{\partial\rho_{\mathrm{c}}}{\partial t}=-R_{\mathrm{c}} \quad \ldots (6)$$

Figure 3 shows the flowchart of the 2D transient model. Eqs. (1)–(6) and the other equations regarding the gas flow and the reaction rate, which can be found in the previous work,[19] were discretized by the finite volume method. The calculation cells in **Fig. 4**(a) were initially adopted, where the origin of the vertical axis is the tuyere level. Each cell involves one set of coke layer and iron ore layer, *i.e.* the material layer set. 32 cells across the height were used to reproduce the actual furnace. Only three cells in the radial direction were adopted to minimize the calculation time while considering the distribution of the ore-to-coke ratio across the radius. The cells at the tuyere level are defined as the raceway cells where the combustion of coke occurs.

The convergence calculation by the implicit method was conducted at each time step with the static calculation cells; that is, the gas flow, the reaction, and the heat transfer were calculated while the solid flow was suspended. This is the reason why the convection terms regarding the solid flow do not appear in Eqs. (2) and (3), while the convection heat transfer by the liquid iron flow is included in Eq. (3). The time step of the calculation was set to five minutes, considering that it takes roughly 15 minutes for the furnace to consume one material layer set.

After the convergence, the following procedure moves the solid downwards, where the calculation cells are updated at each time step so that each cell corresponds to each material layer set. Through this procedure, the number of calculation cells across the height is updated within the range of 30 to 60; therefore the number of calculation cells is between 90 and 180.

1. Return ρ_{c} and ρ_{fe} to the initial values when materials are charged from the furnace top in each cell except the raceway cells, supposing that the apparent coke

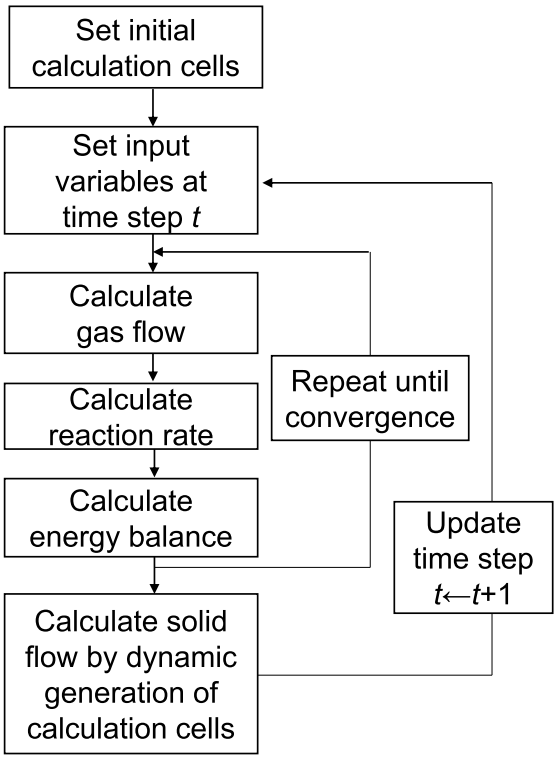

Fig. 3. Flowchart of 2D transient model.

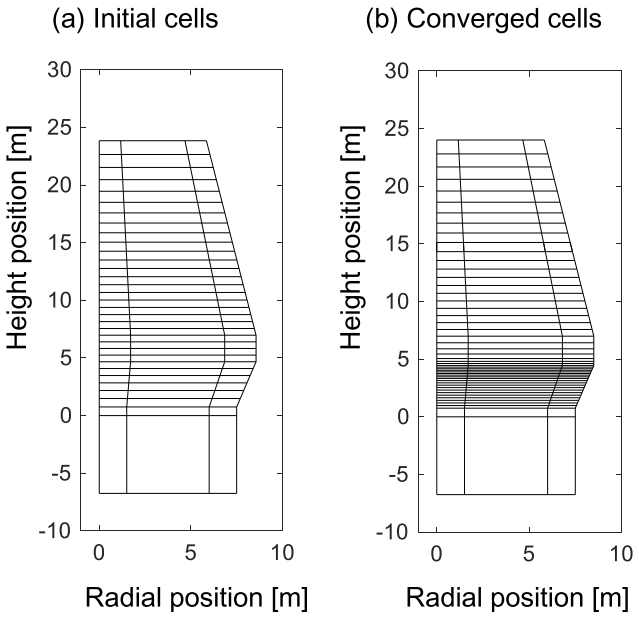

Fig. 4. Calculation cells in developed 2D transient model.

density and iron density in the iron ore are constant.
2. Decrease the volume of each cell while maintaining the mass of coke and iron.
3. Adjust the heights of the three cells at each vertical position so that the heights are the same while keeping the sum of the cell volumes.
4. Change ρ_c and ρ_{fe} of each cell to preserve the mass of coke and iron.
5. Lower all cells by one layer, when the average value of ρ_c in the raceway cells is below its threshold.
6. Load new material layer set from the furnace top to keep the material surface level.

Table 4. Input condition of 2D transient model.

Input variable	Value
Blast volume	6 770 Nm^3/min
PC flow rate	960 kg/min
Blast temperature	1 133°C
Blast moisture	26 g/Nm^3
Enrichment oxygen	284 Nm^3/min
Coke ratio	367 kg/t-pig
Top gas pressure	338 kPa

When the transient model is used for process control, estimation errors are caused by changes in unmeasurable characteristics of the materials and the fluctuation of the gas flow path. In order to incorporate such influence of disturbances into the model, MHE successively updates the three parameters, *i.e.* the coke ratio at the furnace top, the CO gas reduction equilibrium, and the heat-loss, so that the calculated trajectories of the process variables for the past 72 hours coincide with the actual ones.[29)]

2.2. Simulation Result by the Developed 2D Transient Model

Figure 4(b) shows the converged cells at the steady state under the input condition shown in **Table 4**. The ore volume ratios in the center, the intermediate, and the wall regions at the furnace top were set to 0.1, 0.6, and 0.5, respectively. The converged cells below 5 m height shrink because of the coke gasification reaction and the melting of iron ore.

Figures 5(a) and 5(b) shows the steady-state distribution of the iron temperature and the CO gas utilization ratio, *i.e.* the conversion ratio of CO into CO_2, in the height direction at each radial position. Thermal reserve zones are commonly observed in blast furnaces, where the increase rate of the solid temperature becomes gradual around 1 000°C. The thermal reserve zone can be found between 7 and 13 m height in Fig. 5(a), where the non-dimensional radial position r/R is between 0.2 and 1.0. The thermal reserve zone often accompanies a chemical reserve zone, in which the CO gas utilization ratio is close to the equilibrium between Fe and $FeO_{1.05}$.[30,31)] It has been clarified that the chemical reserve zone is crucial to reproduce the actual transition of HMT.[26)] Figure 5(b) indicates that 2D transient model can simulate the chemical reserve zone at the steady state, where the height position is between 9 and 13 m.

Figure 6 shows the simulation result using real plant data, where the vertical axes are mean centered. The upper four figures show the four important input variables and the bottom figure compares the actual HMT (the line with triangles) and the calculated HMT. The dotted line shows the calculation result of the conventional 2D transient model[26)] that employs fixed calculation cells, and the solid line shows that of the developed model in this work.

The operators decreased the blast volume and the PC flow rate and increased CR and BM to ensure the gas permeability from 1.0 day to 1.3 day. Because of the decrease of PC flow rate and the increase of BM, the actual HMT dropped by 60°C from 1.0 day to 1.5 day. The effect of the increase of CR at 1.3 day appeared after the dead time due to the

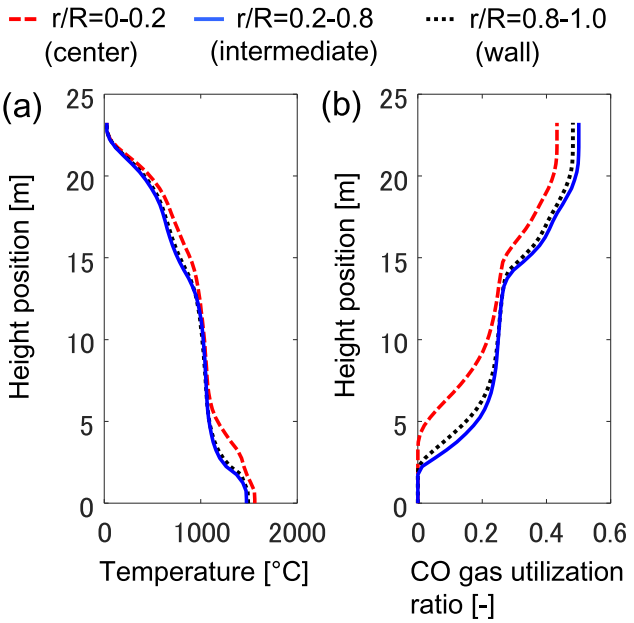

Fig. 5. Calculated steady-state profiles of iron temperature and CO gas utilization ratio in height direction above the tuyere level. (Online version in color.)

material descent, and HMT increased by 100°C from 1.6 day to 2.2 day.

Since the numerical diffusion is caused by the fixed calculation cells, the conventional model cannot capture the sudden change of actual HMT from 1.0 day to 2.2 day. For instance, the calculated HMT is immediately increased by the change of the coke ratio from 1.0 day to 1.3 day because of the numerical diffusion, and it cancels the HMT decrease by the increase of BM and the decrease of PC flow rate. Thus, the change of calculated HMT is smaller than that of actual HMT from 1.2 day to 1.5 day. On the other hand, the developed model successfully simulates the HMT trend. It is because the dynamic generation of the calculation cells suppresses the numerical diffusion and accurately reproduces the dead time of the response of HMT to the change of CR, which has been confirmed with the 1D transient model.[19)]

3. Nonlinear Model Predictive Control

This section describes the details of the nonlinear model predictive control (NMPC) algorithm for reducing the variation of HMT. First, the free response of HMT is predicted

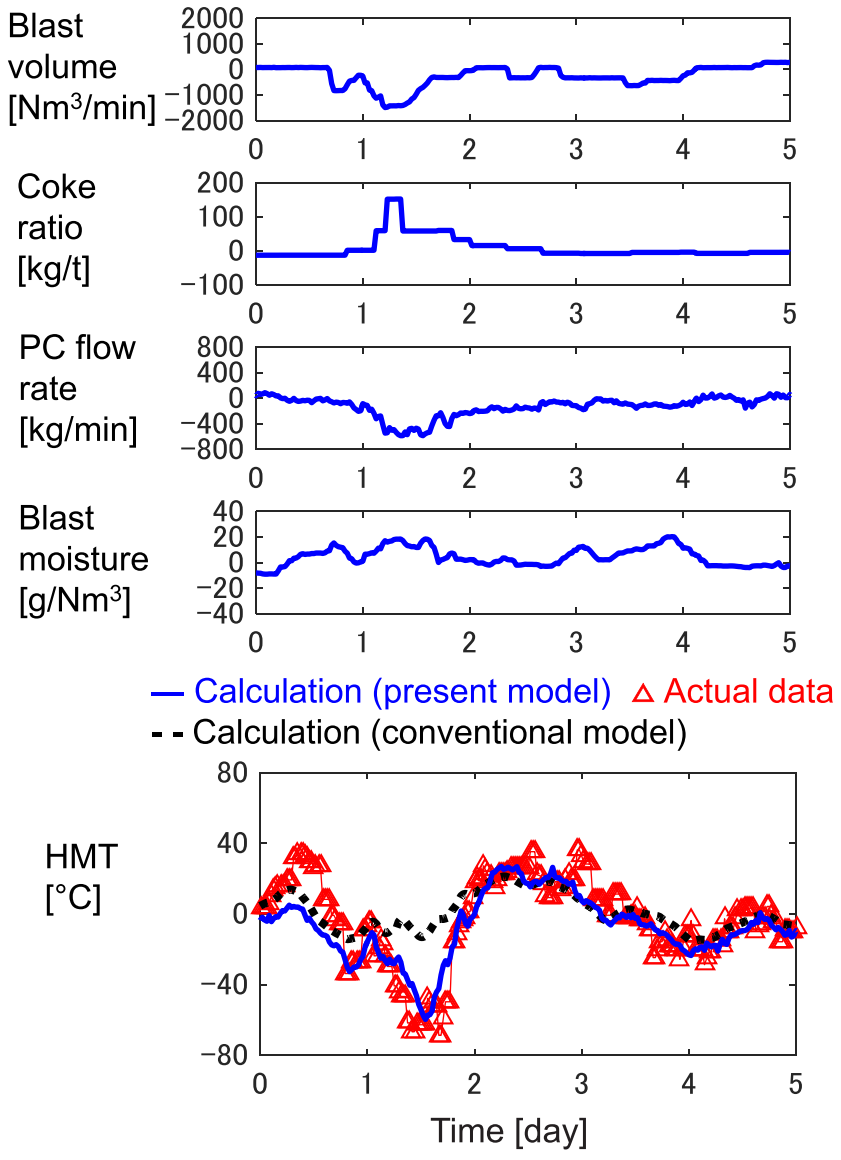

Fig. 6. Comparison of actual HMT and calculated HMT. (Online version in color.)

assuming that the current values of the input variables are maintained in the future. Next, the step response of HMT to the change of the manipulated variable is calculated. Then, an optimum control action for keeping HMT within the target range is determined. The control period is 30 minutes.

3.1. Selection of Manipulated Variable

PCR, BM, and CR are considered as candidates for the manipulated variable. **Table 5** summarizes the dead time of the HMT response to each variable and the operational cost. First, CR was eliminated because of its long dead time and the increase of the operational cost. In general, BM is kept as low as possible to suppress the consumption of RAR. Using BM as the manipulated variable requires to increase the average of BM and results in unnecessary consumption of RAR. Thus, BM is not suitable as the manipulated variable. Although the dead time of PCR is longer than that of BM, PCR is the most cost-effective. Considering above, PCR was chosen as the manipulated variable in this study.

PCR is a crucial index for controlling HMT, and it is calculated by dividing the PC flow rate by the production rate. However, PCR may fluctuate unintentionally since the production rate varies depending on the furnace state. On the other hand, the PC flow rate can be directly manipulated by operators, and it is adjusted to achieve target values of PCR.

3.2. Nonlinear State Space Model

To predict the future HMT and calculate the step response of HMT to the manipulated variable, we introduce the nonlinear state space model whose calculation process is described by

$$\mathbf{x}(t+1) = f(\mathbf{x}(t), \mathbf{u}(t)) \quad \ldots\ldots (7)$$

$$y(t) = C(\mathbf{x}(t-A)) \quad \ldots\ldots (8)$$

where $\mathbf{x}(t)$, $\mathbf{u}(t)$, and $y(t)$ are state variables, input variables, and output variable at time step t, respectively. The nonlinear function f is derived from the 2D transient model described in section 2. There are 15 state variables, which include the temperature, the oxidation degree of iron, and the gas composition in each cell. Seven input variables are listed in Table 1. The output variable is HMT, which is calculated from the iron temperature at the tuyere level by the function C. A is a parameter to describe the residence time of hot metal in the hearth region.

To update the state variables by Eq. (7), the 2D transient model needs to be calculated. The time step for this calculation is five minutes so that the sufficient accuracy is attained. On the other hand, the time step for NMPC can be larger than five minutes because of the sluggish dynamics of the blast furnace. In this work, the time step of the nonlinear state space model was set at 30 minutes by taking account of the trade-off between the accuracy and the computational load. The state variables for six time steps, which are calculated through the 2D transient model, are averaged to derive the state variables in Eq. (7) every 30 minutes (5 min × 6 steps). In addition, the number of cells is dynamically updated within the range between 90 and 180; thus, the number of states is 15 × 90 through 15 × 180. Assuming that the residence time is 2 hours, the parameter A was set to 4 steps.

Table 5. Characteristics of BM, PCR, and CR.

	BM	PCR	CR
Dead time of HMT response	2 hr.	4 hr.	8 hr.
Operational cost	Intermediate	Low	High

3.3. Calculation of Free Response and Step Response

We approximate the future HMT by

$$y(t_0+k) = y_{\text{free}}(t_0+k) + \Delta PCR(t_0) \cdot y_{\text{step}}(k \mid t_0) \quad \ldots\ldots (9)$$

where t_0 denotes the time at which the prediction is conducted. To predict up to ten-hour future, k takes the values from 0 to 19 because it takes approximately 8 hours (16 steps) for the iron to travel from the top furnace to the hearth region. The free response $y_{\text{free}}(t_0+k)$ is calculated by Eqs. (7) and (8), assuming that the input variables at present are kept constant in the future, *i.e.* $\mathbf{u}(t_0+k) = \mathbf{u}(t_0)$. $y_{\text{step}}(k \mid t_0)$ is the step response of HMT to the unit change of PCR at t_0, and $\Delta PCR(t_0)$ is the amount of manipulation at t_0.

Figure 7 shows the example of the free response of HMT. The actual values of the input variables were used to simulate the state variables in the past. Although the actual input variables in the future are not used in the calculation, the predicted transition of HMT agrees with that of actual data. Due to the huge heat capacity of the furnace, the process dynamics is slow, and the HMT shift in 10 hours is substantially affected by the past manipulations and disturbances. On top of that, the actual input variables were kept almost constant in about five hours in this case. Thus, the good

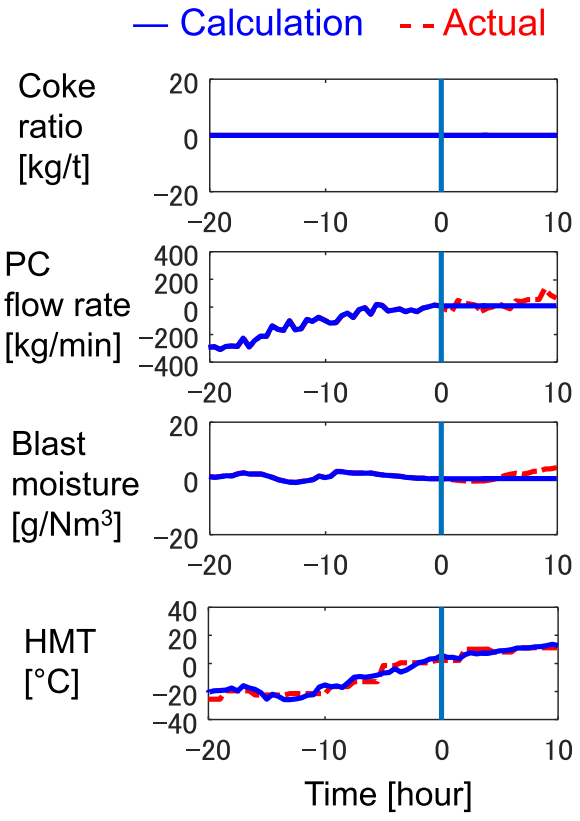

Fig. 7. Prediction of free HMT response using 2D transient model. (Online version in color.)

prediction accuracy was achieved.

The step response of HMT to PCR varies due to the non-linearity of the process. Thus, updating the step response online is necessary to control HMT accurately. First, the trajectory of future HMT $y_{\Delta PC}(t_0+k)$ is predicted by Eqs. (7) and (8), assuming that PCR is increased by 10 kg/t; $\mathbf{u}(t_0+k)=\mathbf{u}(t_0)+\Delta\mathbf{u}$. The operation of increasing the PC flow rate while maintaining the other input variables is represented by $\Delta\mathbf{u}$. The PC flow rate is changed because the input variable of the transient model is not PCR but the PC flow rate. The increased amount of the PC flow rate was calculated by multiplying the PCR change and the current production rate. Subtracting the free response from the predicted HMT response gives the step response of HMT to the increase of PCR.

$$y_{\text{step}}\left(k|t_0\right)=\left(y_{\Delta PC}\left(t_0+k\right)-y_{\text{free}}\left(t_0+k\right)\right)/10 \quad \ldots\ldots (10)$$

The solid line in **Fig. 8**(b) shows the predicted free response of HMT. PC flow rate in Fig. 8(a) and the other input variables are the same with the case of Fig. 7. The dashed line in Fig. 8(b) shows the predicted trajectory of the future HMT when PCR is increased by 10 kg/t. Figure 8(c) shows the step response of HMT to the increase of PCR, which is obtained by subtracting the free response from the predicted HMT response. The small inverse response around 3 hours occurs because the flame temperature at the raceway immediately decreases while RAR, *i.e.* heat source per iron, gradually increases, when PC flow rate is increased.[19)]

3.4. Optimization of Control Action

In the proposed operation guidance system, the operation amount of PCR, *i.e.* ΔPCR, is determined so that HMT falls within the target range in the future while avoiding excessive manipulation as follows.

$$\Delta PCR_{\text{opt}}\left(t_0\right)=\beta\left(\max(y_{\text{free}}\left(t_0+T\right)-y_{\text{U}},0)+\min\left(y_{\text{free}}\left(t_0+T\right)-y_{\text{L}},0\right)\right)\Big/ y_{\text{step}}\left(T|t_0\right) \quad \ldots\ldots (11)$$

where y_{U} and y_{L} are the upper bound and the lower bound of the target range of HMT, which are set to 5°C above and below the set point of HMT, respectively. The parameter T was set to 20, which corresponds to 10 hours. This control law was adopted to reduce the workload of the operators and improve the operators' acceptance of the guidance system, since the operation amount of PCR becomes zero as long as $y_{\text{free}}(t_0+T)$ is within the target range. The relaxation coefficient β was set to 0.4.

4. Evaluation of Operation Guidance System

The operation guidance system using NMPC and MHE was installed in a control room of a blast furnace. **Figure 9** shows an example of the guidance provided to the operators, which is updated every 30 minutes. The guidance system provides the predicted future HMT with or without the recommended control action at the current time, so that the

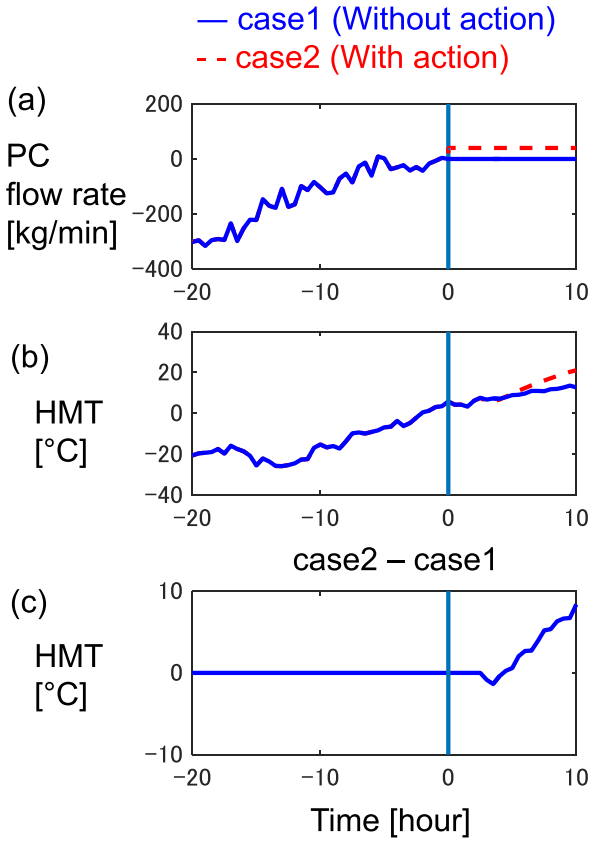

Fig. 8. Calculation of step response of HMT to PCR increase. (Online version in color.)

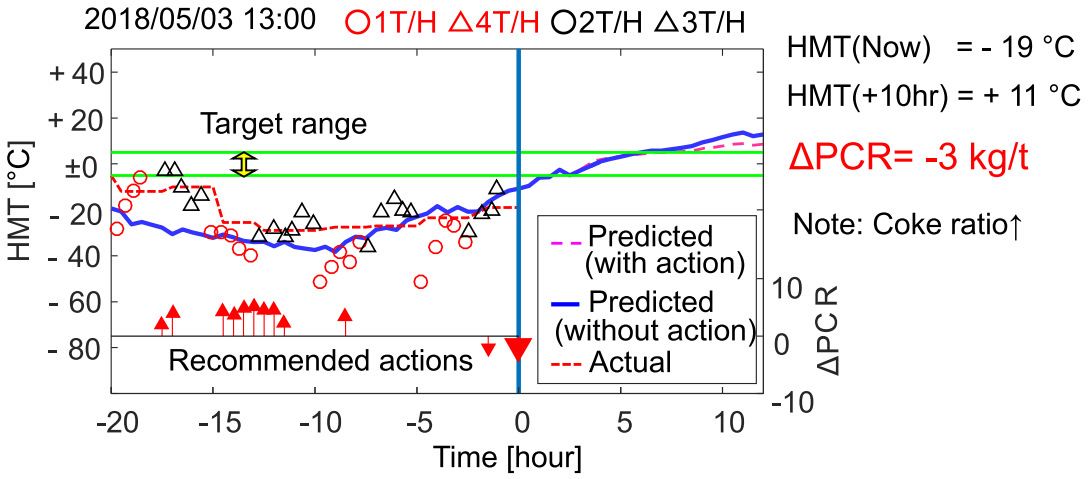

Fig. 9. Example of operation guidance. (Online version in color.)

operators can grasp the effect of the recommended control action. The predicted trajectory of HMT when the recommended control action is executed is calculated by

$$y(t_0+k) = y_{\text{free}}(t_0+k) + \Delta PCR_{\text{opt}}(t_0) \cdot y_{\text{step}}(k|t_0). \quad \ldots (12)$$

The reference information on the disturbances is briefly presented, which improves the operators' approval of the recommended control action. In the case of Fig. 9, even though the current HMT is below the lower bound, reducing PCR by 3 kg/t is suggested because ten-hour-ahead HMT is predicted to exceed the upper bound due to the increase of the coke ratio.

Figure 10 shows the real operation result where the operator changed PCR as recommended by the guidance system and suppressed the control error of HMT successfully. The origin of the vertical axes in the upper three figures are the current values of CR, PCR, and PC flow rate, respectively, whereas the bottom figure shows the deviation from the set point of HMT. The operator decreased CR gradually to reduce the operational cost during the past 20 hours. In response to the decrease of CR, the guidance system predicted that HMT would drop below the set point by more than 20°C and recommended increasing the target value of PCR by 5 kg/t. The operator followed the guidance and manipulated the PC flow rate to increase PCR. Consequently, the actual control error of HMT was successfully suppressed. The recommendation was also consistent with the operators' empirical rule of keeping the constant RAR, *i.e.* the sum of CR and PCR.

Figure 11 shows the operation record for eleven days. The top figure shows HMT which indicates the deviation from the set point. The bottom figure shows the operation amount of PCR, where the bars with the circles denote the actual control actions by the operators and the bars with the triangles denote the recommended ones by the guidance system. The operators mostly followed the guidance and achieved stable HMT compared with Fig. 2, with some exceptions. The operators increased PCR at 4.7 day against the guidance system, which resulted in large errors, more than 30°C, of HMT. Moreover, the operators decreased PCR before 8 day even though the recommended control action by the guidance system was to keep the constant PCR, which resulted in the excessive decrease of HMT. The approval rate of the recommended control action tends to be low when the recommendations are not consistent with the

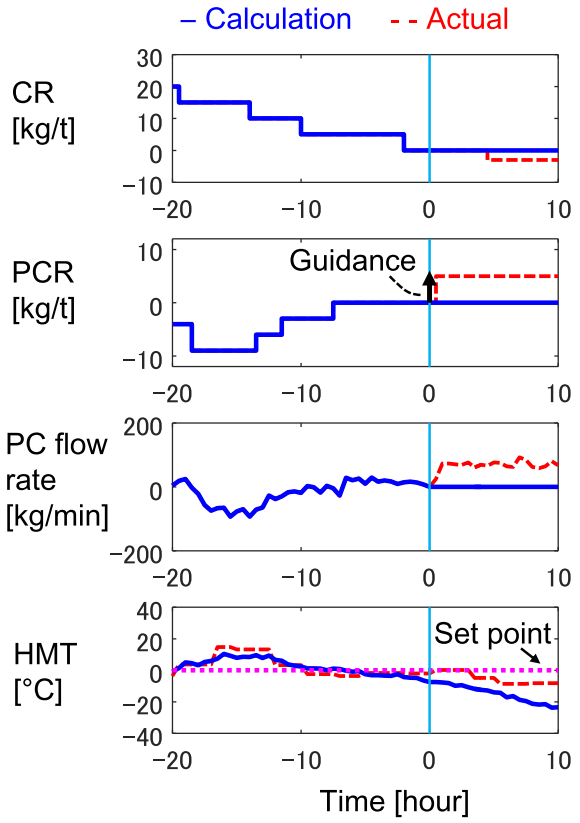

Fig. 10. Real operation result when operators followed guidance. (Online version in color.)

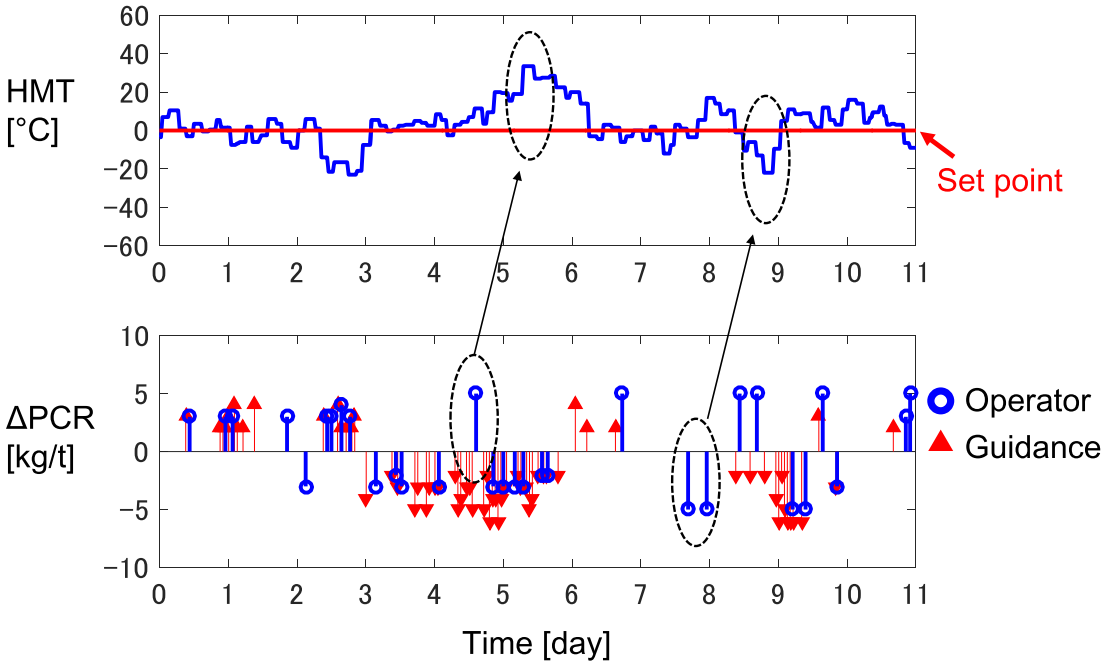

Fig. 11. Comparison of operators' actions and recommended actions. (Online version in color.)

operators' empirical rules that lay emphasis on the thermal indices, *e.g.* the tuyere temperature.

Figure 12 compares the control error of HMT before and after the introduction of the operation guidance system. Operators write the recommended control action on the operation record sheet every hour and decide whether to adopt it. The approval rate of the recommended control actions is around 70%. This result demonstrates the effectiveness of the system that reduces the root mean square (RMS) of the HMT control error by 1.9°C. When HMT gets lower than the target value by 30°C, the operation of increasing coke ratio or decreasing blast volume is performed in the blast furnace to facilitate the slag drainage. Assuming that the lower limit of HMT is 30°C lower than the target value, the decrease of RMS of the control error of HMT by 1.9°C makes it possible to reduce its set point by 2.5°C while keeping the frequency of reaching the lower limit. This decrease in HMT corresponds to the reduction of RAR by 3.0 kg/t. Considering that RAR in recent blast furnace operation is normally between 480 kg/t and 540 kg/t,[32] decreasing RAR by 3.0 kg/t has a huge impact on the reduction of CO_2 emission and the production cost of iron.

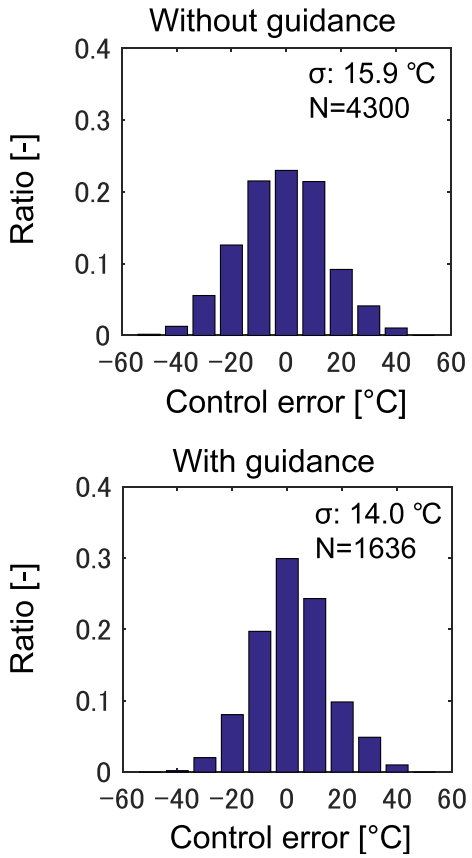

Fig. 12. Control accuracy of HMT. (Online version in color.)

5. Conclusion

To control hot metal temperature (HMT) accurately, an operation guidance system was developed in this study. First, a new 2D transient model for online use that explicitly considers the layer structure of the material was developed. To use the 2D transient model for process control persistently, MHE was adopted, which successively updates model parameters. Furthermore, the operation guidance system was constructed; it provides appropriate PCR control actions based on nonlinear model predictive control. As a result of the online validation in an actual furnace, the effect of reducing the HMT variance by 1.9°C was confirmed.

REFERENCES

1) F. Gagnon, A. Desbiens, É. Poulin, P. Lapointe-Garant and J. S. Simard: *Control Eng. Pract.*, **64** (2017), 88.
2) T. S. Pires, M. E. Cruz, M. J. Colaço and M. A. C. Alves: *Energy*, **149** (2018), 341.
3) R. Bindlish: *Comput. Chem. Eng.*, **73** (2015), 43.
4) M. Niederer, S. Strommer, A. Steinboeck and A. Kugi: *J. Process Control*, **48** (2016), 1.
5) M. Li, Y. Zheng and S. Li: *Ind. Eng. Chem. Res.*, **57** (2018), 12136.
6) S. Shyamal and C. L. E. Swartz: *Ind. Eng. Chem. Res.*, **57** (2018), 13177.
7) L. Ji and J. B. Rawling: *Comput. Chem. Eng.*, **80** (2015), 63.
8) R. D. Martin, F. Obeso, J. Mochon, R. Barea and J. Jimenez: *Ironmaking Steelmaking*, **34** (2007), 241.
9) N. Kaneko, S. Matsuzaki, M. Ito, H. Oogai and K. Uchida: *ISIJ Int.*, **50** (2010), 939.
10) H. Saxen and F. Pettersson: *ISIJ Int.*, **47** (2007), 1732.
11) J. E. Saxen, H. Saxen and H. T. Toivonen: *Appl. Soft Comput.*, **47** (2016), 271.
12) Z. Ding, J. Zhang and Y. Liu: *ISIJ Int.*, **57** (2017), 2022.
13) K. Chen and Y. Liu: *ISIJ Int.*, **57** (2017), 107.
14) X. Tang, L. Zhuang and C. Jiang: *Expert Syst. Appl.*, **36** (2009), 11853.
15) J. Chen: *Eng. Appl. Artif. Intell.*, **14** (2001), 77.
16) J. Zeng, C. Gao and H. Su: *Comput. Chem. Eng.*, **34** (2010), 1854.
17) J. Yagi and I. Muchi: *Trans. Iron Steel Inst. Jpn.*, **10** (1970), 392.
18) M. Hatano, Y. Misaka, Y. Matoba and K. Otsuka: *Trans. Iron Steel Inst. Jpn.*, **22** (1982), 524.
19) Y. Hashimoto, Y. Kitamura, T. Ohashi, Y. Sawa and M. Kano: *Control Eng. Pract.*, **82** (2019), 130.
20) M. Hatano, K. Kurita, H. Yamaoka and T. Yokoi: *Trans. Iron Steel Inst. Jpn.*, **25** (1985), 933.
21) K. Otsuka, Y. Matoba, Y. Kajiwara, M. Kojima and M. Yoshida: *ISIJ Int.*, **30** (1990), 118.
22) D. Fu, Y. Chen, Y. Zhao, J. D'Alessio, K. J. Ferron and C. Q. Zhou: *Appl. Therm. Eng.*, **66** (2014), 298.
23) X. F. Dong, A. B. Yu, S. J. Chew and P. Zulli: *Metall. Mater. Trans. B*, **41** (2010), 330.
24) Y. Shen, B. Guo, S. Chew, P. Austin and A. Yu: *Metall. Mater. Trans. B*, **47** (2016), 1052.
25) K. Yang, S. Choi, J. Chung and J. Yagi: *ISIJ Int.*, **50** (2010), 972.
26) Y. Hashimoto, Y. Sawa, Y. Kitamura, T. Nishino and M. Kano: *ISIJ Int.*, **58** (2018), 1210.
27) J. A. Castro, H. Nogami and J. Yagi: *ISIJ Int.*, **40** (2000), 637.
28) K. Takatani, T. Inada and Y. Ujisawa: *ISIJ Int.*, **39** (1999), 15.
29) Y. Hashimoto, Y. Sawa and M. Kano: *ISIJ Int.*, **59** (2019), 1534.
30) K. Okabe, T. Hamada and A. Watanabe: *Tetsu-to-Hagané*, **55** (1969), 764 (in Japanese).
31) H. Itaya, T. Fukutake, K. Okabe and T. Nagai: *Tetsu-to-Hagané*, **62** (1976), 472 (in Japanese).
32) M. Naito, K. Takeda and Y. Matsui: *Tetsu-to-Hagané*, **100** (2014), 2 (in Japanese).

Practical Operation Guidance on Thermal Control of Blast Furnace

Article *in* ISIJ International · September 2019

DOI: 10.2355/isijinternational.ISIJINT-2019-119

5 authors, including:

Yoshinari Hashimoto
JFE Steel, Japan
11 PUBLICATIONS **35** CITATIONS

SEE PROFILE